Journal of
Materials Chemistry C

RSCPublishing

PAPER

View Article Online
View Journal

Cite this: DOI: 10.1039/c3tc30894d

Tunable electrical memory characteristics of brush copolymers bearing electron donor and acceptor moieties†

Kyungtae Kim,‡[a] Yi-Kai Fang,‡[b] Wonsang Kwon,[a] Seungmoon Pyo,[c]
Wen-Chang Chen*[b] and Moonhor Ree*[a]

A series of brush copolymers bearing *N*-phenylcarbazole (PK) and 2-biphenyl-5-(4-ethoxyphenyl)-1,3,4-oxadiazole (BEOXD) moieties in various compositions were studied in detail, in particular their electrical memory characteristics, optical and electrical properties, morphological structures, and interfaces. Nanoscale thin films of the brush copolymers in devices were found to exhibit excellent unipolar electrical memory versatility, which can easily be tuned by tailoring the chemical composition and by changing the film thickness. Moreover, the molecular orbitals and band gap can be tuned by changing the chemical composition. The novel memory characteristics of these copolymers originate primarily from the cooperative roles of the ambipolar PK and BEOXD moieties, which have different charge trapping and stabilization properties. The electrical memory behaviors were found to occur *via* a favorable hole injection from the electrode and to be governed by trap-limited space-charge limited conduction combined with ohmic conduction and local filament formation. Overall, the brush copolymers are very suitable active materials for the low-cost mass production of high performance, polarity-free digital memory devices that can be operated with very low power consumption, high ON/OFF current ratios, and high stability.

Received 13th May 2013
Accepted 6th June 2013

DOI: 10.1039/c3tc30894d

www.rsc.org/MaterialsC

1 Introduction

Organic materials can be used to fabricate highly integrated electronic devices with simplified manufacturing processes yielding low-cost, flexible, and lightweight devices with three-dimensional stacking that have active device areas approaching the nanoscale.[1–4] Whereas the device fabrication processes and the resistance to the external environment of small-molecule organic materials have limitations,[5–7] polymer materials exhibit easy processability, flexibility, high mechanical strength, and good scalability. Moreover, polymer materials can be processed at low cost and the multi-stack layer structures required for highly dense memory devices can easily be fabricated from them. Several polymers have been reported so far as memory materials.[8–18]

In particular, poly(*N*-vinylcarbazole) has gained attention because of its application in organic electronic devices as a hole transporting layer.[19,20] Oxadiazole-containing polymers have also been extensively investigated as electron-transport materials.[21] Random carbazole and oxadiazole copolymers have been fabricated, with applications in organic light emitting diodes[22–24] and as electrical memory materials.[25] Random copolymers with a high proportion of carbazole moieties exhibit static random access memory (SRAM) behavior, whereas random copolymers with a high proportion of oxadiazole moieties exhibit no electrical memory behavior at all.[25] Controversially, another polymer system containing only oxadiazole moieties has been reported to demonstrate electrical memory characteristics.[26] Nevertheless, the electrical memory characteristics of polymer systems with carbazole and oxadiazole moieties have rarely been investigated. Questions remain about the roles of carbazole and oxadiazole moieties in the electrical memory characteristics of such polymers.

This paper reports the fabrication and electrical properties of programmable memory devices based on a series of brush copolymers containing both carbazole and oxadiazole moieties: poly(9-(4-vinylphenyl)carbazole-*ran*-2-(4-vinylbiphenyl)-5-(4-ethoxyphenyl)-1,3,4-oxadiazole) (PVPK$_m$BEOXD$_n$: m and n are in mol%) (Fig. 1). The brush copolymers' optical and electrochemical properties were measured. The copolymer films' electron densities and interfaces with metal electrodes were

---

[a] *Department of Chemistry, Division of Advanced Materials Science, Center for Electro-Photo Behaviors in Advanced Molecular Systems, Pohang Accelerator Laboratory, Polymer Research Institute, and BK School of Molecular Science, Pohang University of Science & Technology, Pohang 790-784, Republic of Korea. E-mail: ree@postech.edu; Fax: +82-54-279-3399; Tel: +82-54-279-2120*

[b] *Department of Chemical Engineering and Institute of Polymer Science and Engineering, National Taiwan University, Taipei 106, Taiwan. E-mail: chenwc@ntu.edu.tw; Fax: +886-2-3366-5237; Tel: +886-2-3366-5236*

[c] *Department of Chemistry, Konkuk University, Seoul 143-701, Republic of Korea*

† Electronic supplementary information (ESI) available: GIXS data, XR data and analysis results, and *I–V* data. See DOI: 10.1039/c3tc30894d

‡ These authors equally contributed to this work.

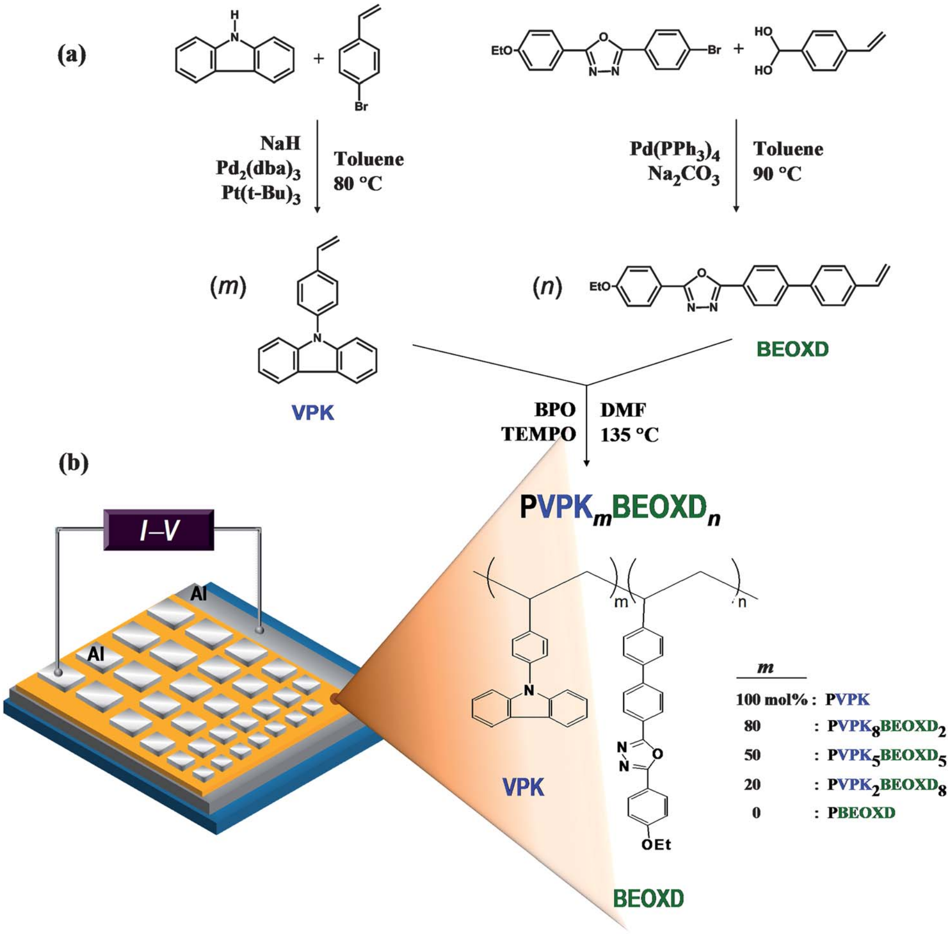

Fig. 1 (a) Synthetic route to *N*-phenylcarbazole (PK) and 2-biphenyl-5-(4-ethoxyphenyl)-1,3,4-oxadiazole (BEOXD) containing brush homopolymers and their copolymers (PVPK$_m$BEOXD$_n$). (b) A schematic diagram of the memory devices fabricated with nanoscale thin films of the PVPK$_m$BEOXD$_n$ copolymers and aluminum (Al) top and bottom electrodes.

examined by synchrotron X-ray reflectivity (XR). Moreover, the brush copolymer films' morphological structures were investigated by synchrotron grazing incidence X-ray scattering (GIXS). These brush copolymers were found to exhibit excellent unipolar electrical memory versatility, which can easily be tuned by tailoring the chemical composition and changing the film thickness. The memory mechanisms were also examined in terms of the molecular orbitals, band gaps, and energy barriers to the work function of the metal electrode of the copolymers.

2 Results and discussion

The optical and electrical properties of the brush copolymers were investigated by UV-vis spectroscopy and cyclic voltammetry (CV) analysis. From the measured UV-vis spectra (Fig. 2a), the band gaps (*i.e.*, the differences between the highest occupied molecular orbital (HOMO) levels and the lowest unoccupied molecular orbital (LUMO) levels) were estimated to be 3.42 eV for PVPK$_8$BEOXD$_2$, 3.40 eV for PVPK$_5$BEOXD$_5$, and 3.37 eV for PVPK$_2$BEOXD$_8$. These band gaps are intermediate between those (3.46 eV and 3.33 eV) of the PVPK and PBEOXD homopolymers, respectively. From the measured CV data (Fig. 2b), the oxidation half-wave potentials ($E_{1/2}$) were determined to be 0.68 V for PVPK$_8$BEOXD$_2$, 0.82 V for PVPK$_5$BEOXD$_5$, and 0.70 V for PVPK$_2$BEOXD$_8$, with respect to the Ag/AgCl standard electrode. In addition, the $E_{1/2}$ values of PVPK and PBEOXD were measured to be 0.51 V and 0.86 V, respectively. $E_{1/2}$ for the external ferrocene/ferrocenium (F_c/F_{c+}) system was measured to be 0.43 V *vs.* Ag/AgCl in acetonitrile. Assuming that the HOMO level for the F_c/F_{c+} standard is −4.80 eV with respect to the zero vacuum level, the HOMO levels were determined to be −5.05 eV for PVPK$_8$BEOXD$_2$, −5.19 eV for PVPK$_5$BEOXD$_5$, and −5.07 eV for PVPK$_2$BEOXD$_8$. Therefore, the LUMO levels were estimated to be −1.63 eV for PVPK$_8$BEOXD$_2$, −1.79 eV for PVPK$_5$BEOXD$_5$, and −1.70 eV for PVPK$_2$BEOXD$_8$. In comparison, the HOMO levels of PVPK and PBEOXD were calculated to be −4.88 eV and −5.23 eV, respectively. From these results, the LUMO levels of PVPK and PBEOXD were determined to be −1.42 eV and −1.90 eV, respectively.

The morphological structures of nanoscale thin films of the brush copolymers were examined by synchrotron GIXS analysis. The PVPK$_8$BEOXD$_2$ copolymer produces featureless two-dimensional (2D) GISAXS and GIWAXS patterns (Fig. 3a and b). Similar GISAXS and GIWAXS patterns were observed for the

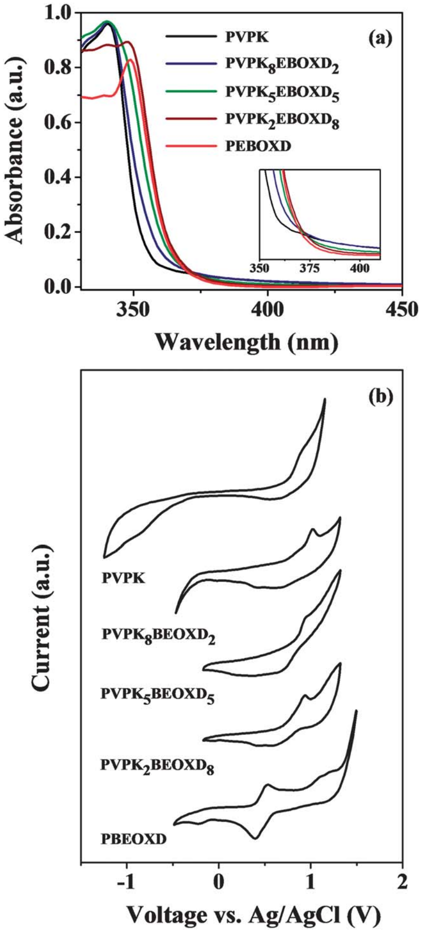

Fig. 2 (a) UV-vis spectra and (b) CV responses of the PVPK and PBEOXD homopolymers and their copolymer films which were coated on quartz substrates and fabricated with Au electrodes supported by silicon substrates, respectively. The inset in (a) shows a magnification of the region around the onset of absorbances. The CV measurements were carried out in aqueous 0.1 M tetrabutylammonium tetrafluoroborate in acetonitrile using an electrochemical workstation (IM6ex impedance analyzer) with a platinum gauze counter electrode and an Ag/AgCl (3.8 M KCl) reference electrode. A scan rate of 100 mV s^{-1} was used.

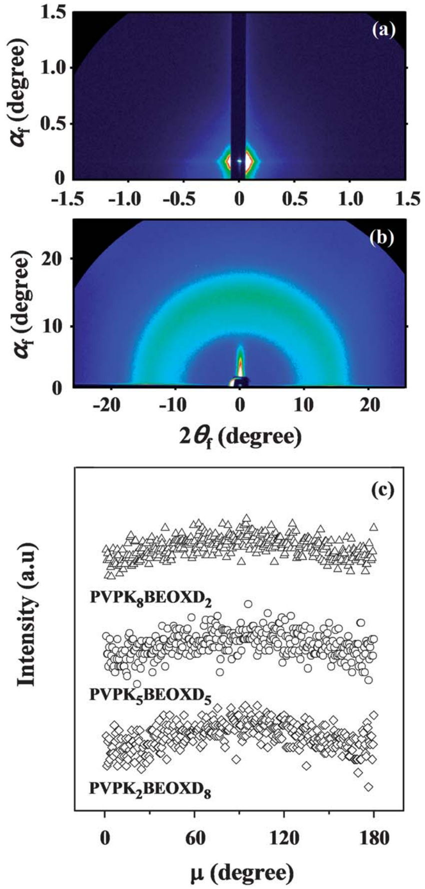

Fig. 3 Synchrotron 2D GIXS patterns of 40 nm thick polymer films measured at 25 °C: (a) 2D GISAXS of a $PVPK_8BEOXD_2$ film measured with $\alpha_i = 0.160°$; (b) 2D GISAXS of a $PVPK_8BEOXD_2$ film measured with $\alpha_i = 0.183°$; (c) azimuthal scattering profiles extracted from the 2D GIWAXS patterns along the amorphous halo ring.

other polymers (Fig. S1 and S2 in the ESI†) as well as for homopolymers. In particular, the GIWAXS patterns contain only one broad, weak amorphous halo scattering ring with a *d*-spacing of approximately 0.50 nm, which corresponds to the mean interdistance of the polymer chains. Note that the amorphous halo scattering ring is slightly anisotropic regardless of the copolymer composition. Thus, the azimuthal scattering profile was extracted from the 2D GISWAXS pattern of each copolymer. The obtained azimuthal scattering profiles are displayed in Fig. 3c as a function of the azimuthal angle μ. All the profiles have a maximum intensity at $\mu = 90°$ and a minimum intensity at $\mu = 0°$ and 180°. These results indicate that for all the nanoscale thin films of the polymers, the polymer chains are oriented preferentially in the film plane rather than randomly; however, their degree of in-plane orientation is not particularly high.

In devices, the polymers are in physical contact with metal electrodes. Thus, the interfaces in the devices were examined by synchrotron XR analysis. Fig. 4a shows the representative XR profiles obtained for three different samples prepared with the $PVPK_8BEOXD_2$ copolymer. Similar XR profiles were observed for the other copolymers (Fig. S3†). As can be seen in Fig. 4a and S3,† all the XR profiles can be satisfactorily fitted with the fitting algorithm proposed by Parratt.[27] The electron density profiles across the thickness direction, as well as other structural parameters, were obtained from these XR analyses. The results are summarized in Fig. 4b, S4–S6† and Table 1.

For the $PVPK_8BEOXD_2$ film coated onto the Si substrate, the XR analysis found that the polymer film has an electron density ρ_e of 371.1 nm^{-3}, a thickness of 39.1 nm, and a surface roughness of 0.2 nm (Table 1). The ρ_e profile across the sample thickness was also determined (Fig. 4b). For the $PVPK_8BEOXD_2$ film coated onto the Al bottom electrode, the XR analysis found that a very thin aluminum oxide layer forms with a thickness of 2.3 nm and a surface roughness of 0.4 nm during the polymer coating process (Table 1 and Fig. S4a†). The top coated polymer film has an electron density of 375.2 nm^{-3} (which is comparable to that of the film prepared on the Si substrate), a thickness of 39.8 nm, and a surface roughness of 0.6 nm. The film surface is rougher than that (0.2 nm) of the film prepared on the Si substrate but not as rough as the Al bottom electrode (1.1 nm).

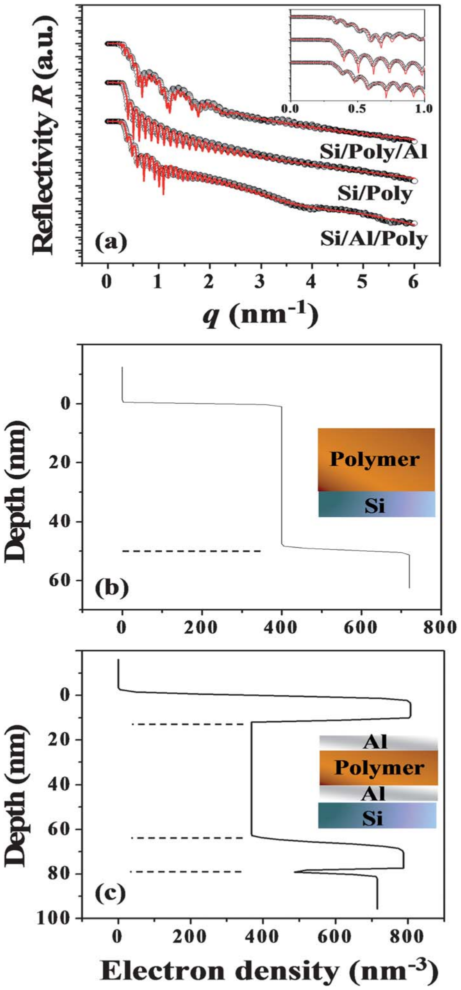

Fig. 4 Synchrotron XR analysis of $PVPK_8BEOXD_2$ films (*ca.* 40 nm thick) in contact with the silicon (Si) substrate, Al bottom electrode, and Al top electrode (*ca.* 10 nm thick): (a) representative XR profiles; (b) electron density profile of the polymer film coated on the Si substrate; (c) electron density profile of the polymer in a Si/Al/polymer/Al structure made by the combination of the electron density profiles (Fig. S4†) determined from the analysis of the XR profiles for the sample specimens of Si/Al/polymer and Si/Polymer/Al structures in (a). In (a), the symbols are the measured data and the solid line represents the fit curve assuming a homogeneous electron density distribution within the film. The inset shows a magnification of the region around the two critical angles: $\alpha_{c,f}$ and $\alpha_{c,s}$ are the critical angles of the film and the substrate (Si or Al electrode), respectively.

Thus, the slightly roughened surface might originate from the rough surface of the Al bottom electrode. These results indicate that a very thin aluminum oxide layer forms on the Al bottom electrode before and/or during the polymer coating process, but aluminum oxide ions and Al atoms do not diffuse from the Al bottom electrode layer into the polymer top layer.

On the other hand, for the Al top electrode deposited onto the polymer film, the Al electrode layer was determined to have a thickness of 11.2 nm, an electron density of 856.3 nm^{-3}, and a roughness of 1.1 nm (Table 1 and Fig. S4b†). An interfacial layer was also found to form with a thickness of 1.3 nm, an electron density of 629.2 nm^{-3}, and a roughness of 0.1 nm. In particular, this interfacial layer's electron density is much higher than that of the polymer but lower than that of Al and furthermore much lower than that of aluminum oxide. The polymer film (bottom layer) was determined to have an electron density of 373.7 nm^{-3} and a roughness of 0.4 nm, which are the same as before the deposition of the Al top layer. These results show that the polymer film surface undergoes no significant damage during the thermal deposition of the Al top electrode. Furthermore, no aluminum oxide layer forms between the polymer film and the Al top electrode; the very thin interfacial layer might be due to the mechanical mixing of the two layers that occurs on the rough surface as well as the nature of Al layer formation *via* thermal deposition.

The XR analyses of the other polymers in equivalent structures yielded results that are similar to those for the $PVPK_8BEOXD_2$ sample specimens, with minor differences in the electron densities of the layers (Table 1, Fig. S5 and S6†). Finally, we combined the XR analysis data for the Al/polymer and polymer/Al samples to produce the whole electron density profiles for the Al/polymer/Al devices shown in Fig. 4c, S5d and S6d.†

In view of these optical and electrochemical properties and morphological and interfacial characteristics, devices with Al/polymer/Al sandwich structures (Fig. 1b) were fabricated with various homopolymer and copolymer film thicknesses and electrically evaluated.

Fig. 5 shows the current–voltage (*I–V*) characteristics of the devices fabricated with 40 nm thick films of the homopolymers and their copolymers. Surprisingly, the PVPK homopolymer was found to immediately reach a low resistance state (*i.e.*, ON-state) very early in the voltage sweep (Fig. 5a); the PVPK film always retains the ON-state in an electric field. In contrast, the PBEOXD homopolymer initially exhibits high resistance (*i.e.*, OFF-state) and no switching behavior during the voltage sweep, *i.e.* it exhibits dielectric characteristics (Fig. 5e). The copolymers also initially enter an OFF-state but exhibit various switching behaviors depending on their chemical composition (Fig. 5b–d).

For the $PVPK_8BEOXD_2$ copolymer, the current undergoes an abrupt increase around +2.4 V in the first positive voltage sweep with a current compliance of 0.01 A, which corresponds to the critical voltage $V_{c,ON}$ to switch on the device (Fig. 5b). This OFF-to-ON transition can function as a "writing" process. Once the device reaches its ON-state, it remains there during the subsequent positive and negative voltage sweeps with a current compliance of 0.01 A or higher and even after the power is turned off. These *I–V* characteristics were also observed in negative voltage sweeps (Fig. S7a†); $V_{c,ON}$ was determined to be −2.9 V. The ON/OFF current ratio is in the 10^7 to 10^{12} range, depending on the turn-on compliance current and the reading voltage; a higher turn-on compliance current and a lower reading voltage result in a higher ON/OFF current ratio. These results indicate that the 40 nm thick $PVPK_8BEOXD_2$ layer in the device exhibits permanent nonvolatile memory behavior, namely unipolar write-once-read-many-times (WORM) memory characteristics.

More interesting memory behaviors were found for the $PVPK_5BEOXD_5$ copolymer. In the positive voltage sweep with a

Table 1 Structural parameters and electron density profiles of various bilayer samples prepared from the polymer film, Si substrate, and Al electrode

Sample	Bottom layer			Polymer layer			Top layer			Interlayer[d]		
(top/bottom)	d^a (nm)	$\rho_e{}^b$ (nm^{-3})	σ^c (nm)	d^a (nm)	$\rho_e{}^b$ (nm^{-3})	σ^c (nm)	d^a (nm)	$\rho_e{}^b$ (nm^{-3})	σ^c (nm)	d^a (nm)	$\rho_e{}^b$ (nm^{-3})	σ^c (nm)
PVK$_8$BEOXD$_2$												
Polymer/Si	—	715.0	0.5	39.1	371.1	0.2				1.8	671.0	0.6
Polymer/Al	11.9	797.3	1.1	39.8	375.2	0.6				2.3	862.7	0.4
Al/polymer				40.8	373.7	0.4	11.2	856.3	1.1	1.3	629.2	0.1
PVPK$_5$BEOXD$_5$												
Polymer/Si	—	718.2	0.9	38.1	378.2	0.2				1.9	637.0	0.5
Polymer/Al	11.4	764.0	0.9	41.8	380.5	0.6				0.6	886.1	0.3
Al/polymer				40.1	378.3	0.2	9.8	797.0	1.1	1.0	695.1	0.9
PVPK$_2$BEOXD$_8$												
Polymer/Si	—	730.3	0.4	26.6	391.8	0.2				0.6	610.0	0.7
Polymer/Al	10.4	871.5	1.2	26.0	385.4	0.6				1.1	892.5	0.1
Al/polymer				26.8	391.8	0.2	9.1	820.1	1.3	1.2	575.2	0.2

[a] Layer thickness. [b] Electron density of the layer. [c] Roughness of the layer in contact with air, lower or upper layer. [d] Silicon oxide layer for Si(bottom)/polymer(top); aluminum oxide layer for Al/polymer; polymer–Al mixed layer (which is due to the roughness of the interface) for polymer/Al systems.

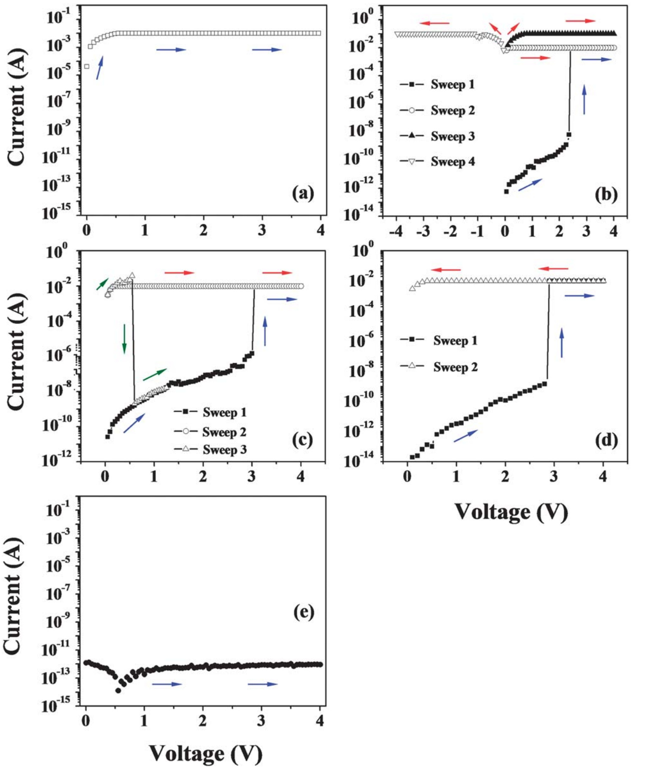

Fig. 5 Typical *I–V* curves of the Al/polymer(40 nm thick)/Al devices, which were measured by voltage sweeps with a compliance current set of 0.01 A: (a) PVPK; (b) PVPK$_8$BEOXD$_2$; (c) PVPK$_5$BEOXD$_5$; (d) PVPK$_2$BEOXD$_8$; (e) PBEOXD. The electrode contact area was 0.5 × 0.5 mm^2. The switching-OFF run in (c) was carried out with a compliance current set of 0.1 A.

current compliance of 0.01 A, the copolymer switches on around +3.0 V ($=V_{c,ON}$), then remains in the ON-state during the subsequent voltage sweeps and even after the power is turned off, and thus exhibits WORM memory characteristics (Fig. 5c). The ON-state was, however, found to return to the OFF-state during voltage sweeps with a higher current compliance (for example, 0.1 A) than that (0.01 A) employed for creating the WORM memory (see the third sweep in Fig. 5c). Similar memory behaviors were observed in the negative voltage sweeps (Fig. S7b†). The ON/OFF current ratio was estimated to be in the 10^5 to 10^8 range, depending on the reading voltage. Overall, the 40 nm thick PVPK$_5$BEOXD$_5$ film in the device exhibits unipolar WORM memory behavior as well as unipolar flash memory characteristics controlled by adjusting the current compliance. These memory behaviors are somewhat different from those of the PVPK$_8$BEOXD$_2$ copolymer.

The PVPK$_2$BEOXD$_8$ copolymer also exhibits interesting electrical memory behavior. The copolymer switches on around +2.8 V ($=V_{c,ON}$) during a positive voltage sweep, but is reset to the OFF-state by a reverse voltage sweep (Fig. 5d). This switching behavior was found to be repeatable. Furthermore, the ON-state returns to the OFF-state when the power is turned off. Similar switching behaviors were observed with $V_{c,ON} = -2.4$ V in the negative voltage sweeps (Fig. S7c†). The ON/OFF current ratio was estimated to be in the 10^6 to 10^{10} range, depending on the reading voltage. These results show that the 40 nm thick PVPK$_2$BEOXD$_8$ film in the device exhibits unipolar DRAM behavior, which is quite different from that of the other copolymers.

Fig. 6 shows the *I–V* data for the devices fabricated with ≥70 nm thick PVPK, PVPK$_8$BEOXD$_2$, and PVPK$_2$BEOXD$_8$ films. The 100 nm thick PVPK film still enters an ON-state under an electric field, as is the case for the 40 nm thick PVPK film discussed above (Fig. 6a). However, the 130 nm thick film exhibits WORM memory behavior; $V_{c,ON}$ is +2.5 V for the PVPK film (Fig. 6b). In contrast, the 70 nm and 100 nm thick PVPK$_8$BEOXD$_2$ films exhibit DRAM behavior (Fig. 6c and d). $V_{c,ON}$ increases from +6.0 V for the 70 nm thick film to +9.1 V for the 100 nm thick film; furthermore, the thicker film has a lower ON/OFF current ratio.

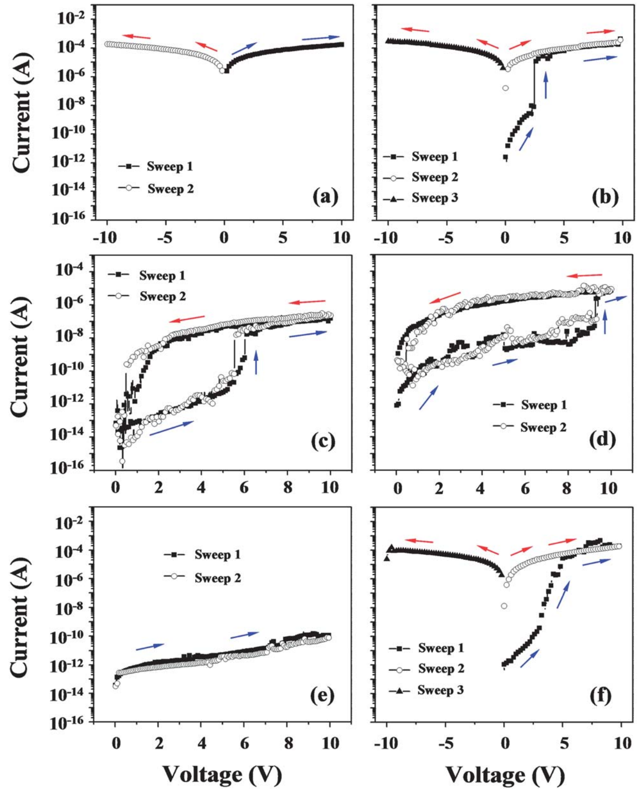

Fig. 6 Typical *I–V* curves of the Al/polymer/Al devices, which were measured by voltage sweeps with a compliance current set of 0.01 A: (a) 100 nm thick PVPK film; (b) 130 nm thick PVPK film; (c) 70 nm thick $PVPK_8BEOXD_2$ film; (d) 100 nm thick $PVPK_8BEOXD_2$ film; (e) 100 nm thick $PVPK_2BEOXD_8$ film; (f) 15 nm thick $PVPK_2BEOXD_8$ film. The electrode contact area was 0.5 × 0.5 mm^2.

These memory characteristics are quite different from the WORM memory characteristics of the 40 nm thick film. On the other hand, a 100 nm thick film of the $PVPK_2BEOXD_8$ copolymer exhibits insulator-like characteristics, with no memory behavior (Fig. 6e). However, this copolymer does surprisingly exhibit WORM memory behavior when its film thickness is 15 nm (Fig. 6f).

Other brush copolymers and the PBEOXD homopolymer were also found to exhibit thickness-dependent *I–V* characteristics. A 70 nm thick film of the $PVPK_5BEOXD_5$ copolymer exhibits DRAM behavior (Fig. 7a), but there is no memory behavior in the 100 nm thick film, which is most likely an insulator (Fig. 7b). Interestingly, the 25 nm thick film exhibits nonvolatile memory behavior but the ON-state cannot be turned off once switched on (*i.e.*, WORM memory behavior) (Fig. 7c), which is a little bit different from the behavior of the 40 nm thick film. In the case of the PBEOXD homopolymer, the 25 nm thick film exhibits the DRAM behavior (Fig. 7d), whereas, interestingly, the 15 nm thick film exhibits WORM memory behavior (Fig. 7e).

Overall, the $PVPK_mBEOXD_n$ copolymer system exhibits both composition- and thickness-dependent memory characteristics (Fig. 8), which are significantly different from the *I–V* characteristics reported previously for copolymers bearing carbazole and oxadiazole derivatives.[25,26] A higher VPK fraction in the copolymer means that a thicker film layer is required in the device to produce electrically bistable switching characteristics. For a copolymer with a given high VPK fraction, thicker films exhibit more stable permanent memory behavior (*i.e.*, WORM memory) whereas films of intermediate thickness exhibit transiently stable memory characteristics (*i.e.*, DRAM); otherwise, thinner films are most likely to be in the ON-state under an electric field, with no memory behavior. On the other hand, a higher BEOXD fraction in the copolymer means that a thinner film layer is required in the device for electrically bistable

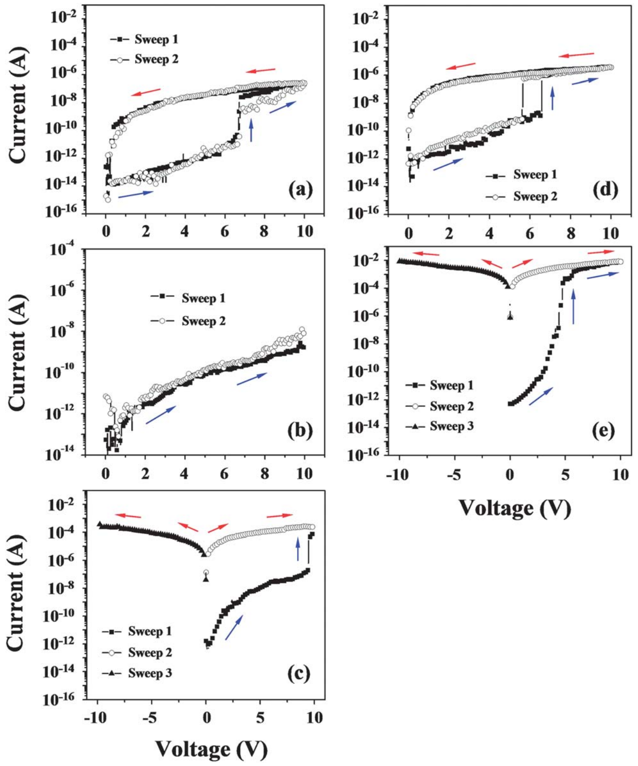

Fig. 7 Typical *I–V* curves of the Al/polymer/Al devices, which were measured by voltage sweeps with a compliance current set of 0.01 A: (a) 70 nm thick $PVPK_5BEOXD_5$ film; (b) 100 nm thick $PVPK_5BEOXD_5$ film; (c) 25 nm thick $PVPK_5BEOXD_5$ film; (d) 25 nm thick PBEOXD film; (e) 15 nm thick PBEOXD film. The electrode contact area was 0.5 × 0.5 mm^2.

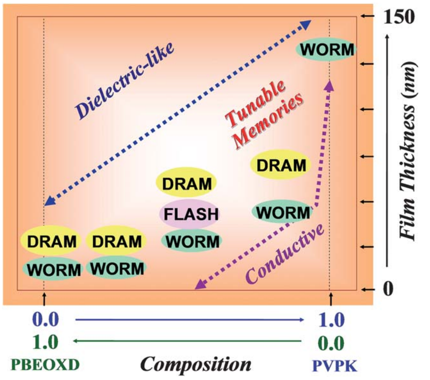

Fig. 8 Composition- and thickness-dependent memory characteristics of the $PVPK_mBEOXD_n$ copolymer system.

switching characteristics to arise. For a copolymer with a high BEOXD fraction, thinner films exhibit more stable permanent memory behavior (*i.e.*, WORM memory) whereas films of intermediate thickness exhibit transiently stable memory characteristics (*i.e.*, DRAM); otherwise, thicker films are most likely to be in the OFF-state, with no memory behavior. In particular, the copolymer with equal proportions of VPK and BEOXD moieties exhibits flash memory behavior in addition to the WORM memory characteristics for films of a certain thickness (40 nm thick).

The stabilities of the devices with 40 nm thick copolymer film layers were tested with a reading voltage of +0.5 V at room temperature in air ambient conditions. Their OFF-states were found to be well retained without any degradation for a test period of 10 h (Fig. S8†). Once the devices based on the $PVPK_8BEOXD_2$ and $PVPK_5BEOXD_5$ copolymers were switched on by applying a voltage of +3.5 V, the ON-states were also found to be well retained without any degradation over the test period (Fig. S8a and b†). Moreover, when the ON state of the $PVPK_5EBOXD_5$ device was switched back to the OFF-state by applying a voltage of 0.3 V with a compliance current of 0.1 A, the OFF-state was again confirmed to persist without any degradation over the whole test period. In the case of the $PVPK_2BEOXD_8$ device, the ON-state was well retained with a continuous voltage bias of +3.5 V (Fig. S8c†). Overall, all of the devices with 40 nm thick copolymer films exhibited excellent reliability even in ambient conditions.

Representative *I–V* data for the devices were further analyzed in detail with various conduction models[28–31] in order to investigate their electrical switching characteristics. Logarithmic plots of the *I–V* data for the devices' OFF-states can be divided into two regimes (Fig. S9†): below and above 1.0 V. For the $PVPK_8BEOXD_2$ and $PVPK_2BEOXD_8$ copolymers, the currents below 1.0 V can be satisfactorily fitted with an ohmic model while those above 1.0 V are well fitted with the trap-limited space-charge limited conduction (SCLC) model. For $PVPK_5BEOXD_5$, the trap-limited SCLC model was found to satisfactorily fit the *I–V* data in both regimes. These results indicate that all the devices in the OFF-state are governed by the trap-limited SCLC mechanism combined with ohmic conduction. On the other hand, for the devices in the ON-state, the *I–V* data were found to be satisfactorily fitted with ohmic conduction (data not shown). Furthermore, their current levels in the ON-state were found to be independent of the device cell size, which is indicative of the formation of heterogeneously localized filaments.

The above results suggest that the memory behaviors of the brush copolymers are governed by trap-limited SCLC combined with ohmic conduction and local filament formation. The charge trapping sites required by these electrical switching mechanisms might arise from the chemical components of the copolymers. For the PVPK homopolymer and the copolymers, the *N*-phenylcarbazole (PK) moiety in the side group mimics both conventional carbazole and triphenylamine, which are well known as hole transporting groups, and can thus be classified as an electron donor. The PK moiety can trap holes on the electron-rich nitrogen atom and stabilize the trapped holes with the aid of its aromatic rings. The vinyl backbone can also be classified as an electron donor because of its hydrocarbon nature, although it might not have the capability to stabilize trapped charges, with only a very weak power to trap holes. However, due to its electron donor characteristics, the vinyl backbone could positively assist the hole trapping and stabilization of the PK moieties. On the other hand, for the PBEOXD homopolymer and copolymers, the oxadiazole moiety in the side group is known to be an electron transporting group and can thus be classified as an electron acceptor, which can trap and stabilize electrons. The biphenyl and phenyl linkers in the side group are known to be electron deficient, however, their electron affinities are not high enough. Thus, they can be classified as weak electron acceptors. However, they are aromatic and indeed can positively assist the electron trapping and stabilization of the oxadiazole moiety. In contrast, the electron donor characteristics of the vinyl backbone and the ethoxy end of the side group could negatively affect the oxadiazole moiety's electron trapping and stabilization. Thus, the PK and BEOXD side groups can effectively act as charge-trapping sites. Therefore, the copolymers have a dual functionality and can trap holes and electrons and stabilize the trapped charges in a certain level, depending on their chemical composition. Under an electrical field (*i.e.*, an applied voltage), charges are trapped in trapping sites. The charge-trapped sites are localized throughout the entire copolymer film layers and are then stabilized in a certain level, and can act as stepping stones for charge flow, namely current flow. When the charge-trapped sites are localized with an interdistance of 1.0 nm or less as stepping stones in the copolymer film layers, current flow can take place favorably between the electrodes in the device *via* the film layer. Thus, under an electric field, local filaments are formed from such charge-trapped sites that enable current flow through the hopping process and result in an ON-state.

For the devices with Al electrodes ($\Phi = -4.28$ eV), the energy barriers to hole injection from the electrode to the active polymer film layer (HOMO level) were estimated to be 0.60 eV for PVPK, 0.95 eV for PBEOXD, 0.77 eV for $PVPK_8BEOXD_2$, 0.91 eV for $PVPK_5BEOXD_5$, and 0.79 eV for $PVPK_2BEOXD_8$. The energy barriers to electron injection from the electrode to the polymer film layer (LUMO level) were estimated to be 2.86 eV for PVPK, 2.38 eV for PBEOXD, 2.65 eV for $PVPK_8BEOXD_2$, 2.49 eV for $PVPK_5BEOXD_5$, and 2.58 eV for $PVPK_2BEOXD_8$. The energy barrier to hole injection is lower than that for electron injection for all the homopolymers and copolymers. Therefore, these results suggest that the conduction processes in the devices are dominated by hole injection.

The ordering of the energy barriers to hole injection in the films is PVPK < $PVPK_8BEOXD_2$ < $PVPK_2BEOXD_8$ < $PVPK_5BEOXD_5$ < PBEOXD, as discussed above. One might, therefore, expect that the ordering of the $V_{c,ON}$ values would be PVPK < $PVPK_8BEOXD_2$ < $PVPK_2BEOXD_8$ < $PVPK_5BEOXD_5$ < PBEOXD. As discussed above, the copolymers' electrical switching behaviors were, however, found to further depend on the VPK and BEOXD fractions (*i.e.*, chemical composition) as well as on the film layer thickness. Thus, the prediction of the $V_{c,ON}$ values cannot be based only on the energy barriers. Furthermore, it is very difficult to rationalize the relationships of the $V_{c,ON}$ values with the energy barriers, chemical compositions, film thicknesses, and other associated factors.

In view of the BEOXD unit's electron acceptor characteristics, one might expect that the PBEOXD homopolymer and the copolymers with a large BEOXD fraction can more favorably trap electrons, leading to electron injection based conduction processes in their devices. Considering the higher energy barrier to electron injection from the electrode to the polymer film layer discussed above, such conduction processes should require higher $V_{c,ON}$ values. However, $V_{c,ON}$ was found not to be simply proportional to the BEOXD fractions in the polymers. This result suggests that such electron injection based conduction processes might not take place in the devices based on the copolymers; if such a conduction process takes place at a certain electric field, it may occur in a very minor portion rather than a major portion. Namely, hole injection based conduction processes were confirmed to be more favorable for the devices based on the BEOXD-rich copolymers.

In fact, the oxadiazole moiety's electron affinity originates from the electron deficiency generated by its heterocyclic conjugation ring and further from the ability to stabilize trapped electrons by delocalization into the heterocyclic conjugation ring. In the case of the BEOXD unit, electron deficiency and stabilization power are enhanced somewhat by the electron deficient characteristics of the additional phenyl and biphenyl linkers, as discussed above. However, the oxadiazole moiety contains lone pairs of electrons on the oxygen and nitrogen atom components. In addition, the ethoxy end group is an electron donor with a further two lone pair electrons. Taking these facts into account, the BEOXD unit might also have an affinity for holes and be able to stabilize them. Therefore, the BEOXD unit can act as an electron trapping site as well as a hole trapping site, depending on circumstances. Of course, its capacity for hole trapping and stabilization is weaker than its capacity for electron trapping and stabilization and, furthermore, weaker than the PK unit's capacity for hole trapping and stabilization. Nevertheless, thinner films of the PBEOXD homopolymer and the BEOXD-enriched copolymers exhibit excellent DRAM and WORM memory behaviors in devices. These results confirm that the BEOXD moieties in the homopolymer and copolymers are ambipolar and thus can trap holes, which results in current flows under the appropriate conditions.

The various observed *I–V* characteristics might indeed be primarily due to differences between the charge trapping and stabilization powers of the PK and BEOXD units in the PVPK$_m$BEOXD$_n$ copolymers. Taking these factors into account, the observed film thickness dependent memory behaviors suggest that the efficiency of the local filament based conduction process is a function of the travel path distance (*i.e.*, the conduction path length) in the copolymer layer between the top and bottom electrodes. The local filament based conduction path length is longer in the PK-enriched copolymers and so can provide charge-trapping sites with higher capacity and stabilization power. In other words, thicker films of the PK-enriched copolymer can exhibit electrical memory behaviors. In contrast, the local filament based conduction path length is shorter in the BEOXD-enriched copolymer, which can provide charge-trapping sites with lower capacity and stabilization power. Thus, only thinner films of the BEOXD-enriched copolymers exhibit electrical memory behaviors.

3 Conclusions

A series of brush copolymers bearing *N*-phenylcarbazole (PK) and 2-biphenyl-5-(4-ethoxyphenyl)-1,3,4-oxadiazole (BEOXD) moieties (PVPK$_m$BEOXD$_n$ copolymers) were investigated in detail, in particular their electrical memory characteristics, optical and electrical properties, morphological structures, and interfaces. In nanoscale thin films, the copolymers are amorphous but have a tendency to orient in the film plane. In the devices, the brush copolymer films were found to be in contact with the Al top and bottom electrodes without diffusion of the metal atoms and ions. The HOMO (−4.88 to −5.23 eV) and LUMO (−1.42 to −1.90 eV) levels and the band gaps (3.33 to 3.46 eV) of the copolymers can be tuned by tailoring their compositions.

The excellent electrical memory versatility of the nanoscale copolymer layers in the devices with the Al top and bottom electrodes can be tuned by tailoring the chemical composition and the film layer thickness: unipolar DRAM, flash memory, and WORM memory characteristics were all demonstrated, including conductor-like and insulator-like behaviors. These novel memory characteristics originate from the cooperative roles of the ambipolar PK and BEOXD moieties, which have significantly different charge trapping and stabilization powers; despite their ambipolarities, the PK moiety has a higher affinity to holes whereas the BEOXD moiety has a higher affinity to electrons. The electrical memory behaviors were found to occur *via* a favorable hole injection from the electrode and further to be governed by trap-limited space-charge limited conduction (SCLC) combined with ohmic conduction and local filament formation.

Overall, this study has demonstrated that PVPK$_m$BEOXD$_n$ copolymers are suitable active materials for the low-cost mass production of high performance, polarity-free digital memory devices that can be operated with very low power consumption, high ON/OFF current ratios, and high stability. Moreover, the memory modes of these copolymers can easily be tuned by changing the composition and film thickness.

4 Experimental

2,2,6,6-Tetramethylpiperidine-1-oxyl (TEMPO) and benzoyl peroxide (BPO) were obtained from Acros (Geel, Belgium). $Pd(PPh_3)_4$ and sodium carbonate were purchased from Strem Chemicals (Newburyport, MA, USA) and Showa (Tokyo, Japan), respectively. Anhydrous toluene and dimethylformamide (DMF) were purchased from TEDIA (Fairfield, CT, USA). Tetrabutylammonium perchlorate (TBAP) was obtained from TCI (Tokyo, Japan). Other chemicals were purchased from Aldrich (Milwaukee, WI, USA). All the chemicals were used as received unless otherwise noted. TBAP was purified by recrystallization twice from ethyl acetate and then dried under vacuum prior to use.

2-(4-Bromophenyl)-5-(4-ethoxyphenyl)-1,3,4-oxadiazole was synthesized (Fig. 1a), according to the method reported in the literature.[31] The obtained compound (10.36 g, 30.0 mmol) and 4-vinylphenylboronic acid (5.33 g, 36.0 mmol) were reacted together with the aid of $Pd(PPh_3)_4$ (1.23 g, 1.05 mmol) and Na_2CO_3 (3.81 g, 30.0 mmol) in a mixture of toluene (210 mL), ethanol (6 mL) and deionized distilled water (30 mL) at 90 °C under a nitrogen atmosphere for 16 h. After the completion of the reaction, the mixture was cooled down to room temperature and filtered. The solvent was removed by evaporation under a reduced pressure to obtain a crude product. The product was purified by column chromatography on a silica gel column using dichloromethane as an eluent, washed with methanol (twice), and dried under vacuum at 70 °C to afford 7.44 g (67%) of the target monomer, 2-(4-vinylbiphenyl)-5-(4-ethoxyphenyl)-1,3,4-oxadiazole (BEOXD), as a green powder. The obtained BEOXD monomer was characterized by proton nuclear magnetic resonance (^{1}H NMR) spectroscopy using a Bruker NMR spectrometer (model Avance 300 MHz FT-NMR, Fällanden, Switzerland). ^{1}H NMR (300 MHz, $CDCl_3$, δ (ppm)): 1.46 (t, 3H), 4.13 (q, 2H), 5.31 (d, 1H, ArCH═CH *cis*), 5.83 (d, 1H, ArCH═CH *trans*), 6.79 (dd, 1H, ArCH═CH), 7.01 (d, 2H), 7.51 (d, 2H), 7.62 (d, 2H), 7.74 (d, 2H), 8.06 (d, 2H), 8.17 (d, 2H).

On the other hand, 9-(4-vinylphenyl)carbazole (VPK) was synthesized (Fig. 1b), according to the method in the literature report.[32]

From the above BEOXD and VPK monomers, a series of brush copolymers were synthesized in various compositions *via* nitroxide-mediated free radical polymerization (NMFRP) (Fig. 1a), and further purified by Soxhlet extraction in acetone. The obtained brush copolymers were finally dried under vacuum at 60 °C for 1 day: PVPK ($\overline{M_w} = 12\,000$ and PDI = 1.30; $T_g = 210$ °C and $T_d = 405$ °C), PVPK$_8$BEOXD$_2$ (77.5 mol% VPK and 22.5 mol% BEOXD; $\overline{M_w} = 9900$ and PDI = 1.23; $T_g = 202$ °C and $T_d = 368$ °C), PVPK$_5$BEOXD$_5$ (49.6 mol% VPK and 50.4 mol % BEOXD; $\overline{M_w} = 10\,000$ and PDI = 1.31; $T_g = 197$ °C and $T_d = 377$ °C), PVPK$_2$BEOXD$_8$ (14.0 mol% VPK and 86.0 mol% BEOXD; $\overline{M_w} = 10\,800$ and PDI = 1.27; $T_g = 193$ °C and $T_d = 389$ °C), and PBEOXD ($\overline{M_w} = 14\,200$ and PDI = 1.38; $T_g = 176$ °C and $T_d = 406$ °C) (Fig. 1).

All the obtained polymers and their compositions were characterized in $CDCl_3$ by ^{1}H NMR spectroscopy (300 MHz). Weight-average weights ($\overline{M_w}$) and polydispersity indices (PDI) were determined by gel permeation chromatography (GPC) using a Lab Alliance RI2000 instrument (Shah Alam, Malaysia; one column, MIXED-D from Polymer Laboratories, Amherst, MA, USA) connected with a refractive index detector (Schambeck SFD Gmbh, Bad Honnef, Germany) which was calibrated with polystyrene standards. All GPC analyses were performed using tetrahydrofuran (THF) eluent at a flow rate of 1 mL min^{-1} at 40 °C. Glass transition and degradation temperatures (T_g and T_d) were measured by differential scanning calorimetry (DSC) and thermogravimetry (TGA), respectively. DSC measurements were performed under a nitrogen atmosphere at a heating rate of 20 °C min^{-1} using a TA instrument DSC-Q100 (New Castle, DE, USA) while TGA analysis was carried out at a heating rate of 20 °C min^{-1} under a nitrogen atmosphere using a PerkinElmer Pyris 1 TGA (Waltham, MA, USA). All the polymers were found to be soluble in common solvents such as chloroform, THF, toluene, chlorobenzene, dichlorobenzene, and dimethylacetamide.

Devices were fabricated as follows. For each polymer, homogeneous solutions with two different concentrations (0.7 and 1.0 wt%) were prepared in chloroform, followed by filtrations through PTFE-membrane micro filters with a pore size of 0.2 μm. Aluminum (Al) bottom electrodes with a thickness of 300 nm were deposited on precleaned silicon (Si) substrates by electron-beam evaporation. Each polymer solution was spin-coated onto the Al bottom electrodes at 2000 rpm for 40 s, followed by drying at 80 °C under vacuum for 1 day. The resulting films' thicknesses were determined using a spectroscopic ellipsometer (model M2000, Woollam, Lincoln, NE, USA). Then, Al top electrodes were thermally evaporated onto the polymer films at a pressure of *ca.* 10^{-6} torr through a shadow mask. The resulting top electrodes had a thickness of 300 nm and the area varied from 2.0 mm × 2.0 mm to 0.5 mm × 0.5 mm.

For XR experiments, three kinds of sample specimens were prepared for each brush copolymer: (i) polymer films (40 nm thick) on the Si substrates with a native oxide layer, (ii) polymer films (30 nm thick) on 10 nm thick Al-deposited Si substrates (here, the Al layer was deposited by electron-beam evaporation), and (iii) thermally evaporated Al films (10 nm thick) on 30 nm thick polymer films coated onto the Si substrates. Synchrotron XR measurements were performed at the 3D and 8D beamlines of the Pohang Accelerator Laboratory (PAL).[33] A Si(111) double-crystal monochromator was used to select a wavelength λ of 0.1541 nm within an energy resolution of $\Delta\lambda/\lambda = 5 \times 10^{-4}$, and a Sagittal bender for the second crystal was used to focus the X-ray beam in the horizontal direction. The primary beam was defined by four slits before the sample, and another two slits were used as receiving slits after the sample. The beam was collimated at the sample position to 2 mm (horizontal) by 0.1 mm (vertical). The measured reflected intensity was normalized to the intensity of the primary beam, which was monitored with an ionization chamber. Specular reflection was measured in the θ–2θ scanning mode. The reflectivity R, *i.e.* the ratio of the reflected beam intensity to the primary beam intensity, was measured down to just above 10^{-8}. To obtain accurate determinations of the critical angles of the silicon substrate and of the thin film, 2θ was scanned at small increments of 0.01° at angles smaller than 1.0°. At higher angles, the step width was increased to 0.02–0.1°. The obtained data underwent data binning, geometrical correction, and the background subtraction procedure described in the literature.[33,34]

GIXS measurement was performed at the PAL 3C beamline.[35,36] Measurements were performed at a sample-to-detector distance (SDD) of 125 mm for grazing incidence wide-angle X-ray scattering (GIWAXS) and 2220 mm for grazing incidence small-angle X-ray scattering (GISAXS). Scattering data were typically collected for 30 s using an X-ray radiation source of $\lambda = 0.138$ nm with a two-dimensional charge-coupled detector (Roper Scientific, Trenton, NJ, USA). The incidence angle α_i of the X-ray beam was set at 0.183° for wide angle scattering and 0.160° for small-angle scattering, which is between the critical angle of the polymer films and the silicon substrate

($\alpha_{c,f}$ and $\alpha_{c,s}$). Scattering angles were corrected according to the positions of the X-ray beams reflected from the silicon substrate with respect to a pre-calibrated silver behenate (TCI, Tokyo, Japan) powder. Aluminum foil pieces were applied as a semi-transparent beam stop because the intensity of the specular reflection from the substrate was much stronger than the scattering intensity of the polymer films near the critical angle.

I–V characteristics of the devices were tested under ambient air conditions using a Keithley 4200 semiconductor analyzer (Cleveland, OH, USA). *I–V* curves were recorded by performing forward and reverse voltage scans between −4.0 V and +4.0 V at a scan rate of 500 mV s^{-1}. Optical properties were measured using a Scinco ultraviolet-visible (UV-vis) spectrometer (model S-3100, Seoul, Korea). Cyclic voltammetry (CV) measurements were carried out in a 0.1 M solution of tetrabutylammonium tetrafluoroborate in acetonitrile by using an electrochemical workstation (IM6ex impedance analyzer, Zahner, Kronach, Germany) with a platinum gauze counter electrode and an Ag/AgCl (3.8 M KCl) reference electrode, and the polymers were coated onto the Au bottom electrode, which was deposited on a silicon wafer. A scan rate of 100 mV s^{-1} was used.

Acknowledgements

This study was supported by the National Research Foundation (NRF) of Korea (Doyak Program 2011-0028678 and the Center for Electro-Photo Behaviors in Advanced Molecular Systems (2010-0001784)) and the Ministry of Science, ICT & Future Planning (MSIP) (World Class University Program (R31-2008-000-10059-0) and BK21 Program). Synchrotron GIXS and XR measurements were supported by MSIP, POSCO and POSTECH Foundation. The work at National Taiwan University was supported by the National Science Council under the contract number, NSC 98-2221-E-002-006-MY3.

References

1 Q. D. Ling, D.-J. Liaw, C. Zhu, D. S.-H. Chan, E.-T. Kang and K.-G. Neoh, *Prog. Polym. Sci.*, 2008, **33**, 917.

2 K. S. Kwok and J. C. Ellenbogen, *Mater. Today*, 2002, **5**, 28; J. C. Scott, *Science*, 2004, **304**, 62.

3 Z. Bao, A. J. Lovinger and A. Dodabalapur, *Appl. Phys. Lett.*, 1996, **69**, 3066; S. Choi, S. Hong, S. H. Cho, S. Park, S. M. Park, O. Kim and M. Ree, *Adv. Mater.*, 2008, **20**, 1766.

4 Y. Yang, J. Ouyang, L. Ma, R. J. Tseng and C. Chu, *Adv. Funct. Mater.*, 2006, **16**, 1001.

5 A. R. Elsharkawi and C. Kao, *J. Phys. Chem. Solids*, 1977, **38**, 95; C. Chiang, *Solid State Commun.*, 1981, **39**, 111.

6 H. J. Gao, K. Sohlberg, Z. Q. Xue, H. Y. Chen, S. M. Hou, L. P. Ma, X. W. Fang, S. J. Pang and S. J. Pennycook, *Phys. Rev. Lett.*, 2000, **84**, 1780; Z. J. Donhauser, B. A. Mantooth, K. F. Kelly, L. A. Bumm, J. D. Monnell, J. J. Stapleton, D. W. Price Jr, A. M. Rawlett, D. L. Allara, J. M. Tour and P. S. Weiss, *Science*, 2001, **292**, 2303; J. Chen and D. Ma, *Appl. Phys. Lett.*, 2005, **87**, 23505; C.-H. Tu, Y.-S. Lai and D.-L. Kwong, *Appl. Phys. Lett.*, 2006, **89**, 062105.

7 D. Kolosov, D. S. English, V. Bulovic, P. F. Barbara, S. R. Forrest and M. E. Thompson, *J. Appl. Phys.*, 2001, **90**, 3242.

8 D. Ma, M. Aguiar, J. A. Freire and I. A. Hümmelgen, *Adv. Mater.*, 2000, **12**, 1063.

9 S. Baek, D. Lee, J. Kim, S.-H. Hong, O. Kim and M. Ree, *Adv. Funct. Mater.*, 2007, **17**, 2637; D. Lee, S. Baek, M. Ree and O. Kim, *Jpn. J. Appl. Phys.*, 2008, **47**, 5665; D. Lee, S. Baek, M. Ree and O. Kim, *Electron. Lett.*, 2008, **44**, 596; Y.-S. Lai, C.-H. Tu, D.-L. Kwong and J. S. Chen, *Appl. Phys. Lett.*, 2005, **87**, 122101; Y.-S. Lai, C.-H. Tu, D.-L. Kwong and J. S. Chen, *IEEE Electron Device Lett.*, 2006, **27**, 451.

10 T. J. Lee, S. Park, S. G. Hahm, D. M. Kim, K. Kim, J. Kim, W. Kwon, Y. Kim, T. Chang and M. Ree, *J. Phys. Chem. C*, 2009, **113**, 3855.

11 H. S. Majumdar, A. Bandyopadhyay, A. Bolognesi and A. J. Pal, *J. Appl. Phys.*, 2002, **91**, 2433; E. Y. H. Teo, Q. D. Ling, Y. Song, Y. P. Tan, W. Wang, E. T. Kang, D. S. H. Chan and C. Zhu, *Org. Electron.*, 2006, **7**, 173.

12 S. L. Lim, Q. Ling, E. Y. H. Teo, C. X. Zhu, D. S. H. Chan, E.-T. Kang and K. G. Neoh, *Chem. Mater.*, 2007, **19**, 5148.

13 Q. Ling, Y. Song, S. J. Ding, C. Zhu, D. S. H. Chan, D.-L. Kwong, E.-T. Kang and K. G. Neoh, *Adv. Mater.*, 2005, **17**, 455; L.-H. Xie, Q.-D. Ling, X.-Y. Hou and W. Huang, *J. Am. Chem. Soc.*, 2008, **130**, 2120; M. Karakawa, M. Chikamatsu, Y. Yoshida, R. Azumi, K. Yase and C. Nakamoto, *Macromol. Rapid Commun.*, 2007, **28**, 1479; S. K. Majee, H. S. Majumdara, A. Bolognesi and A. J. Pal, *Synth. Met.*, 2006, **156**, 828; T.-W. Kim, K. Lee, S.-H. Oh, G. Wang, D.-Y. Kim, G.-Y. Jung and T. Lee, *Nanotechnology*, 2008, **19**, 405201.

14 Q.-D. Ling, D.-J. Liaw, E. Y.-H. Teo, C. Zhu, D. S.-H. Chan, E.-T. Kang and K.-G. Neoh, *Polymer*, 2007, **48**, 5182.

15 S. G. Hahm, S. Choi, S.-H. Hong, T. J. Lee, S. Park, D. M. Kim, W.-S. Kwon, K. Kim, O. Kim and M. Ree, *Adv. Funct. Mater.*, 2008, **18**, 3276.

16 D. M. Kim, S. Park, T. J. Lee, S. G. Hahm, K. Kim, J. C. Kim, W. Kwon and M. Ree, *Langmuir*, 2009, **25**, 11713; K. Kim, S. Park, S. G. Hahm, T. J. Lee, D. M. Kim, J. C. Kim, W. Kwon, Y.-G. Ko and M. Ree, *J. Phys. Chem. B*, 2009, **113**, 9143; T. J. Lee, C.-W. Chang, S. G. Hahm, K. Kim, S. Park, D. M. Kim, J. Kim, W.-S. Kwon, G.-S. Liou and M. Ree, *Nanotechnology*, 2009, **20**, 135204.

17 S. Park, K. Kim, D. M. Kim, W. Kwon, J. Choi and M. Ree, *ACS Appl. Mater. Interfaces*, 2011, **3**, 765; S. Park, K. Kim, J. C. Kim, W. Kwon, D. M. Kim and M. Ree, *Polymer*, 2011, **52**, 2170; S. G. Hahm, T. J. Lee, D. M. Kim, W. Kwon, Y.-G. Ko, T. Michinobu and M. Ree, *J. Phys. Chem. C*, 2011, **115**, 21954.

18 S. G. Hahm, N.-G. Kang, W. Kwon, K. Kim, Y.-G. Ko, S. Ahn, B.-G. Kang, T. Chang, J.-S. Lee and M. Ree, *Adv. Mater.*, 2012, **24**, 1062; D. M. Kim, Y.-G. Ko, J. K. Choi, K. Kim, W. Kwon, J. Jung, T.-H. Yoon and M. Ree, *Polymer*, 2012, **53**, 1703; T. J. Lee, Y.-G. Ko, H.-J. Yen, K. Kim, D. M. Kim, W. Kwon, S. G. Hahm, G.-S. Liou and M. Ree, *Polym. Chem.*, 2012, **3**, 1276; Y.-G. Ko, W. Kwon, D. M. Kim, Y.-S. Gal and M. Ree, *Polym. Chem.*, 2012, **3**, 2028; Y.-G. Ko, W. Kwon, H.-J. Yen,

C.-W. Chang, D. M. Kim, K. Kim, S. G. Hahm, T. J. Lee, G.-S. Liou and M. Ree, *Macromolecules*, 2012, **45**, 3749; K. Kim, H.-J. Yen, Y.-G. Ko, C.-W. Chang, D. M. Kim, W. Kwon, S. G. Hahm, G.-S. Liou and M. Ree, *Polymer*, 2012, **53**, 4135.

19 W. W. Chung and C. L. Hong, *Macromolecules*, 2006, **39**, 7232.

20 (*a*) G. Wang, C. Yuan, H. Wu and Y. Wei, *J. Appl. Phys.*, 1995, **78**, 2679; (*b*) S. Jerzy, B. Dariusz, W. Marek and B. Adam, *Chem. Mater.*, 2002, **14**, 89.

21 A. Kraft, A. C. Grimsdale and A. B. Holmes, *Angew. Chem., Int. Ed.*, 1998, **37**, 402; D. Y. Kim, H. N. Cho and C. Y. Kim, *Prog. Polym. Sci.*, 2000, **25**, 1089; L. Akcelrud, *Prog. Polym. Sci.*, 2003, **28**, 875.

22 P. Wang, C. Chai, Q. Yang, F. Wang, Z. Shen, H. Guo, X. Chen, X. Fan, D. Zou and Q. Zhou, *J. Polym. Sci., Part A: Polym. Chem.*, 2008, **46**, 5452.

23 D. D. Evanoff Jr, J. B. Carroll, R. D. Roeder, Z. J. Hunt, J. R. Lawrence and S. H. Foulger, *J. Polym. Sci., Part A: Polym. Chem.*, 2008, **46**, 7882.

24 K. Tsuchiya, K. Sakaguchi, A. Kawakami, H. Taka, H. Kita, T. Shimomura and K. Ogino, *Synth. Met.*, 2010, **160**, 1679.

25 Y.-K. Fang, C.-L. Liu and W.-C. Chen, *J. Mater. Chem.*, 2011, **21**, 4778.

26 W. Kwon, B. Ahn, D. M. Kim, Y.-G. Ko, S. G. Hahm, Y. Kim, H. Kim and M. Ree, *J. Phys. Chem. C*, 2011, **115**, 19355.

27 L. G. Parratt, *Phys. Rev.*, 1954, **95**, 359.

28 P. Mark and W. Helfrich, *J. Appl. Phys.*, 1962, **33**, 205.

29 A. J. Campell, D. D. C. Bradley and D. G. Lidzey, *J. Appl. Phys.*, 1997, **82**, 6326.

30 K. L. Jessen, *J. Vac. Sci. Technol., B: Microelectron. Nanometer Struct.–Process., Meas., Phenom.*, 2003, **21**, 1528; J. Frenkel, *Phys. Rev.*, 1938, **54**, 647; C. Laurent, E. Kay and N. Souag, *J. Appl. Phys.*, 1988, **64**, 336.

31 G. Liu, Q.-D. Ling, E. Y. H. Teo, C.-X. Zhu, D. S.-H. Chan, K.-G. Neoh and E.-T. Kang, *ACS Nano*, 2009, **3**, 1929; C. Ye, Q. Ping, M. Li, J. Luo, Z. Tang, J. Pei, J. Chen, Z. Shuai, L. Jiang and Y. Song, *J. Am. Chem. Soc.*, 2012, **134**, 20053.

32 L. Deng, P. T. Furuta, S. Garon, J. Li, D. Kavulak, M. E. Thompson and J. M. J. Fréchet, *Chem. Mater.*, 2006, **18**, 386.

33 J. Bolze, M. Ree, H. S. Youn, S.-H. Chu and K. Char, *Langmuir*, 2001, **17**, 6683; Y. Hwang, K. Heo, C. H. Chang, M. K. Joo and M. Ree, *Thin Solid Films*, 2006, **510**, 159.

34 F. Salah, B. Harzallah and A. van der Lee, *J. Appl. Crystallogr.*, 2007, **40**, 813.

35 J. Yoon, K.-W. Kim, J. Kim, K. Heo, K. S. Jin, S. Jin, T. J. Shin, B. Lee, Y. Rho, B. Ahn and M. Ree, *Macromol. Res.*, 2008, **16**, 575; B. Lee, Y.-H. Park, Y. Hwang, W. Oh, J. Yoon and M. Ree, *Nat. Mater.*, 2005, **4**, 147; B. Lee, W. Oh, Y. Hwang, Y.-H. Park, J. Yoon, K. S. Jin, K. Heo, J. Kim, K.-W. Kim and M. Ree, *Adv. Mater.*, 2005, **17**, 696.

36 J. Yoon, K. S. Jin, H. C. Kim, G. Kim, K. Heo, S. Jin, J. Kim, K.-W. Kim and M. Ree, *J. Appl. Crystallogr.*, 2007, **40**, 476; J. Yoon, S. W. Lee, S. Choi, K. Heo, K. S. Jin, S. Jin, G. Kim, J. Kim, K.-W. Kim, H. Kim and M. Ree, *J. Phys. Chem. B*, 2008, **112**, 5338; G. Kim, S. Park, J. Jung, K. Heo, J. Yoon, H. Kim, I. J. Kim, J. R. Kim, J. I. Lee and M. Ree, *Adv. Funct. Mater.*, 2009, **19**, 1631.